The Regional Climate-Chemistry-Ecology Coupling Model RegCM-Chem (v4.6)-YIBs (v1.0): Development and Application

Nanhong Xie[1], Tijian Wang[1]*, Xiaodong Xie[2], Xu Yue[2], Filippo Giorgi[3], Qian Zhang[1], Danyang Ma[1], Rong Song[1], Beiyao Xu[1], Shu Li[1], Bingliang Zhuang[1], Mengmeng Li[1], Min Xie[1], Natalya Andreeva Kilifarska[4], Georgi Gadzhev[5], Reneta Dimitrova[6]

[1]School of Atmospheric Sciences, Nanjing University, Nanjing, 210023, China

[2]School of Environmental Sciences and Engineering, Nanjing University of Information Science and Technology, Nanjing, 210023, China

[3]Earth System Physics Section, the Abdus Salam International Centre for Theoretical Physic, Trieste, 34100, Italy

[4]Climate, Atmosphere and Waters Research Institute, Bulgarian Academy of Sciences, Sofia, 1113, Bulgaria

[5]National Institute of Geophysics, Geodesy and Geography, Bulgarian Academy of Sciences, Sofia, 1113, Bulgaria

[6]Department of Meteorology and Geophysics, Faculty of Physics, Sofia University, Sofia, 1113, Bulgaria

Corresponding to: Tijian Wang (tjwang@nju.edu.cn)

Abstract. The interactions between the terrestrial biosphere, atmospheric chemistry, and climate involve complex feedbacks that have traditionally been modeled separately. We present a new framework that couples the Yale Interactive terrestrial Biosphere (YIBs), a dynamic plant-chemistry model, with the RegCM-Chem model. RegCM-Chem-YIBs integrates meteorological variables and atmospheric chemical composition from RegCM-Chem with land surface parameters from YIBs. The terrestrial carbon flux calculated by YIBs, are fed back into RegCM-Chem interactively, thereby representing the interactions between fine particulate matter ($PM_{2.5}$), ozone (O_3), and carbon dioxide (CO_2). For testing purposes, we carry out a one-year simulation (2016) at a 30 km horizontal resolution over East Asia with RegCM-Chem-YIBs. The model accurately captures the spatio-temporal distribution of climate, chemical composition, and ecological parameters. In particular, the estimated O_3 and $PM_{2.5}$ are consistent with ground observations, with correlation coefficients (R) of 0.74 and 0.65, respectively. The simulated CO_2 concentration is consistent with observations from six sites (R ranged from 0.89 to 0.97) and exhibits a similar spatial pattern when compared to carbon assimilation products. RegCM-Chem-YIBs produces reasonably good gross primary productivity (GPP) and net primary productivity (NPP), showing seasonal and spatial distributions consistent with satellite observations, and mean biases (MBs) of 0.13 and 0.05 kg C m^{-2} year^{-1}. This study illustrates that the RegCM-Chem-YIBs is a valuable tool to investigate coupled interactions between the terrestrial carbon cycle, atmospheric chemistry, and climate change at a higher resolution in regional scale.

1 Introduction

Air pollution and climate change are major focal points in atmospheric and environmental science (Hong et al., 2019; Kan et al., 2012). In this respect, China exhibits both high air pollution levels and large greenhouse gas emissions (Zheng et al., 2018; Li et al., 2016a). The consequences of China's air pollution on global, regional, and urban climate are significant (Liu et al., 2022; Lu et al., 2020). Conversely, global warming impacts the dynamics, physics, and chemical mechanisms underlying atmospheric pollutant formation, underscoring a robust link between atmospheric chemistry and climate change (Baklanov et al., 2016; Fiore et al., 2015; Fiore et al., 2012).

$PM_{2.5}$, O_3, and CO_2 are important for regional air pollution and climate. O_3, a potent pollutant, is harmful for human health and can also harm chloroplasts in plant cells, consequently influencing the carbon assimilation efficiency of land ecosystems (Xie et al., 2019; Ainsworth et al., 2012). Similarly, $PM_{2.5}$ is not only one of the most dangerous pollutants for human health (Kim et al., 2015), but also affects atmospheric radiation mechanics, modulates radiation fluxes reaching vegetation canopies, and hence impacts plant physiological processes and terrestrial carbon fluxes (Lu et al., 2017; Strada and Unger, 2016). Terrestrial ecosystems, absorbing nearly 30% of anthropogenic CO_2 emissions, play an essential role in the global carbon cycle, for which even minor alterations can trigger significant oscillations in atmospheric CO_2 concentrations, potentially destabilizing the global climate (Forkel et al., 2016; Ahlstrom et al., 2015). As a result, $PM_{2.5}$, O_3, and CO_2 exhibit intricate interplays.

Models that couple climate and chemistry are vital tools for investigating the interplay between environmental pollution and climate warming (Dunne et al., 2020; Yahya et al., 2017), and in particular the direct and indirect influences of aerosols, O_3, and greenhouse gases on climates at different scales (Chutia et al., 2019; Pu et al., 2017; Li et al., 2017a). For example, the Atmospheric Chemistry and Climate Model Intercomparison Project (ACCMIP) addresses this issue through the use of a range of global coupled climate-chemistry models (Young et al., 2013; Shindell et al., 2013; Lamarque et al., 2013). In fact, China has achieved significant advancements in atmospheric chemistry and coupled climate models during recent years, both at the global and regional scale. Representative models encompass BCC_AGCM2.0_CAM, BCC-AGCM_CUACE2.0, RIEMS-Chem, and RegCCMS.

BCC_AGCM2.0_CAM was coupled by the China Meteorological Administration through direct integration of the National Climate Center's atmospheric circulation model (BCC-AGCM) with the Canadian aerosol model (CAM) (Zhang et al., 2012). Atmospheric model BCC-AGCM2.0 was developed by the National Climate

62   Center. For example, at the regional scale the Institute of Atmospheric Physics of the Chinese Academy of Sci-

63   ences, has constructed the Regional Integrated Environmental Modeling System (RIEMS), which is widely used

64   in studies on East Asian regional climate change and severe weather systems (Scheuch et al., 2015; Xiong et al.,

65   2009). It incorporates atmospheric chemistry and aerosol dynamics into the Regional Integrated Environment

66   Modeling System and produces online simulations of meteorological parameters, aerosol chemical composition,

67   optical characteristics, radiation forcing, and aerosol-induced climate feedback (Li et al., 2014; Li et al., 2013a;

68   Han et al., 2012).

69   The Nanjing University developed the Regional Climate Chemistry Modeling System (RegCCMS), a syn-

70   thesis of the regional climate model RegCM2 and the tropospheric atmospheric chemistry model TACM, pri-

71   marily oriented toward investigating the spatio-temporal distribution, radiation forcing, and climatic effects of

72   tropospheric O_3 and sulfate aerosols. Subsequently, RegCM3 was coupled with TACM, integrating modules for

73   aerosols into RegCCMS (Zhang et al., 2014; Li et al., 2009). The system incorporates parameterization schemes

74   facilitating the simulation of aerosols' direct, indirect, and semidirect climatic effects. Extensive evaluations

75   have been carried out regarding major aerosol impacts on the meteorology and regional climate within East Asia

76   (Zhuang et al., 2013; Zhuang et al., 2011; Wang et al., 2010). Subsequently, Shalaby et al. (2012) developed the

77   regional climate-chemistry model RegCM-Chem, by coupling the CBM-Z gas phase chemistry module to ver-

78   sion 4 of the RegCM system, RegCM4 (Giorgi et al., 2012). RegCM-Chem also includes a simplified aerosol

79   scheme including radiatively interactive sulfates, carbonaceous aerosols, sea salt, and desert dust (Zakey et al.,

80   2006; Solmon et al., 2006), and it has been used for a variety of applications in different domains.

81   By developing the regional climate-chemistry-ecology model RegCM-Chem-YIBs, in which the interactive

82   biosphere model YIBs is coupled to RegCM-Chem. The model can produce multi-process simulations of re-

83   gional climate, atmospheric chemistry, and ecology, especially $PM_{2.5}$, O_3, and CO_2, and their interactions with

84   atmospheric variables (Xu et al., 2023; Ma et al., 2023b; Ma et al., 2023a; Xu et al., 2022; Gao et al., 2022; Xie

85   et al., 2020). Here we expand on these previous studies. We carry out a one-year simulation (2016) at a 30 km

86   horizontal resolution over East Asia with RegCM-Chem-YIBs and conduct a comprehensive assessment. We

87   validate the simulation not only in terms of atmospheric variables but also in terms of atmospheric composition

88   and ecological parameters, by comparison with a range of observations available for this period.

89   The paper is organized as follows. In section 2 we first describe the RegCM-Chem-YIBs system, focusing

90   in particular on the newly implemented coupling with the ecological component. We also describe the observa-

91   tion datasets used in the model assessment. The simulations are then analyzed in section 3, while section 4 pre-

92   sents our conclusions and a general discussion of our results and future developments.

93   **2 Model and Methods**

94   **2.1 Overall Framework**

95   In RegCM-Chem-YIBs, the atmospheric variables produced by RegCM (temperature, humidity, precipita-

96   tion, radiation, etc.) and atmospheric chemical compounds, such as O_3 and $PM_{2.5}$, produced by the chemis-

97   try/aerosol module are input into YIBs, which simulates the physiological processes of vegetation (such as pho-

98   tosynthesis, respiration, etc.), and calculates land process variables such as CO_2 fluxes, BVOC emissions, and

99   stomatal conductance. The output from YIBs is then fed back to RegCM-Chem, which adjusts the CO_2, O_3, and

100   $PM_{2.5}$ concentrations and their radiative and microphysical effects on the meteorological fields in the lower at-

101   mosphere, thereby achieving a full coupling between climate, chemistry, and ecology. Figure 1 shows the basic

102   framework of the RegCM-Chem-YIBs coupled model.
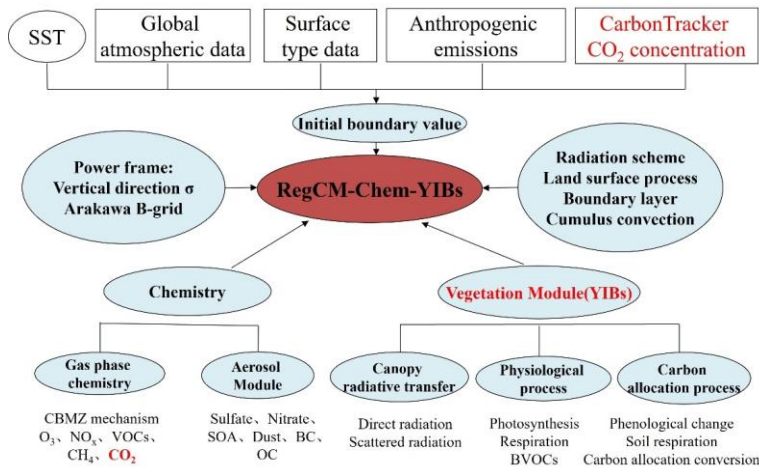
103

104   **Figure 1.** RegCM-Chem-YIBs Coupling Model Framework

105   **2.2 Descriptions of the RegCM-Chem model**

106   The inception of the RegCM system traces back to the late 1980s and early 1990s, when NCAR's (U.S. Na-

107   tional Center for Atmospheric Research) RegCM 1 was first developed for climate downscaling (Giorgi, 1990;

108   Giorgi and Bates, 1989; Dickinson et al., 1989). After a series of developments, subsequent versions were in-

109   troduced, such as RegCM2 (Giorgi et al., 1993), RegCM2.5 (Giorgi and Mearns, 1999), RegCM3 (Pal et al.,

110   2007), RegCM4 (Giorgi et al., 2012). The RegCM system presently managed, maintained, and expanded by the

111   Earth System Physics (ESP) section of the Abdus Salam International Center for Theoretical Physics (ICTP), is

112   open-source and extensively employed in regional climate studies, contributing to the establishment of a com-

113   prehensive Regional Climate Research Network (RegCNET) (Giorgi et al., 2006). The model can be applied to

114   all regions of the globe (Giorgi et al., 2012) and is moving into a fully-coupled regional Earth system model

115   framework through coupling with the ocean (Turuncoglu et al., 2013; Artale et al., 2010), lake (Small et al.,

116   1999), aerosol (Solmon et al., 2006), dust (Zakey et al., 2006), chemistry (Shalaby et al., 2012), hydrology

117   (Coppola et al., 2003), land surface processes (Oleson et al., 2008). Of specific interest for our study, Shalaby et

118   al. (2012) added a radiatively interactive gas-phase chemical module (CBM-Z) to RegCM4, generating

119   RegCM-Chem, in which atmosphere physics and chemistry are fully coupled.

120   **2.2.1 Aerosol Mechanisms**

121   The RegCM model integrates a simplified aerosol framework, enabling the simulation of sulfate, black

122   carbon (BC), organic carbon (OC), sea salt, and desert dust. The model specifies an external mix of aerosols and

123   accounts for the influence of horizontal advection, turbulent diffusion, vertical transport, emissions, dry and wet

124   deposition, and gas-liquid transition on aerosol concentration (Solmon et al., 2012; Giorgi et al., 2012; Zakey et

125   al., 2006). The secondary organic aerosol scheme VBS (volatile basis set) has also been introduced into the

126   model to further improve RegCM-Chem's simulation of tropospheric aerosols (Yin et al., 2015). The model in-

127   corporates the ISORROPIA thermodynamic equilibrium scheme to describe the formation process of secondary

128   inorganic salts, thus enhancing the model's capability to simulate secondary inorganic aerosols (Li et al., 2016b).

129   The further addition of bioaerosols was carried out by Liu (Liu et al., 2016).

130   **2.2.2 Gas phase chemical mechanism**

131   RegCM4-Chem includes the CBM-Z (Carbon Bond Mechanism-Z) atmospheric chemistry mechanism

132   (Zaveri and Peters, 1999). The CBM-IV mechanism, recognized for its widespread use, serves as the basis for

133   CBM-Z (Gery et al., 1989) and was developed to balance simulation accuracy and computational speed. Both

134   CBM-IV and CBM-Z categorize volatile organic compounds (VOCs) into groups dependent on their carbon

bond formation and use lumped species to represent each group. However, CBM-Z includes additional species and reactions compared to CBM-IV, which are crucial for simulating typical urban environments and long-term simulations at regional to global scales. Enhancements in CBM-Z include (1) specific representation of stable alkanes; (2) updated parameters for higher alkanes; (3) separation of olefins into two categories based on differing reactions; (4) addition of peroxy alkane self-reactions significant in low-NOx, such as remote regions; (5) incorporation of reactions among alkanes, peroxyacyl radicals, and NO_3, which are crucial nocturnally; (6) inclusion of long-lived organic nitrates and peroxides; and (7) refinement of isoprene and its peroxy radical chemistry. Collectively, these updates to the CBM-Z chemistry mechanism enhance the model's ability to more accurately simulate long-lived VOCs and address the atmospheric chemistry transition from urban to rural settings.

2.2.3 Radiation scheme

RegCM4 adopts the CCM3 radiation scheme, which uses the delta-Eddington approximation for solar spectral radiation and accounts for the attenuation effect of atmospheric components such as O_3, H_2O, CO_2, O_2 on solar radiation (Kiehl et al., 1996). The CCM3 radiation scheme, implemented in RegCM4, extends from 0.2 to 5 μm, and is segmented into 18 bands. It uses the cloud scattering and absorption parameter scheme, and cloud optical characteristics. As cumulus clouds form, the cloud optical characteristics stretch from the cloud base up to the cloud top, and the radiation calculations assume random overlap. It is assumed in the model that the cloud thickness is equivalent to that of the model's vertical layers, with distinctive cloud water and ice contents assigned to high, middle, and low clouds (Slingo, 1989).

2.2.4 Photolysis rate

Meteorological conditions and chemical input fields determine the photolysis rate, with most variables dynamically produced by the RegCM's modules and updated every 3-30 minutes. SO_2 and NOx, inverted from the US standard atmosphere's vertical profile, are model-defined. Owing to the computational demands of precise photolysis rates from the Tropospheric Ultraviolet–Visible Model (TUV) method (Madronich and Flocke, 1998) and eight data stream spherical harmonics discretization, a look-up table and interpolation method are adopted. Considering the significant impact of clouds on the photolysis rate, it becomes crucial to adjust the cloud amount. Here we use the cloud optical depth information for each grid cell within the model. As the absorption and scattering of ultraviolet radiation by clouds reduce the photolysis rate inside and below the cloud

162 while enhancing it above the cloud, the correction value for the photolysis rate under clear sky conditions de-

163 pends on the position to the cloud layer. Hence, cloud height and optical depth are necessary for the photolysis

164 rate computation (Chang et al., 1987).

165 **2.2.5 Deposition Processes**

166   In the model, dry deposition serves as the principal removal process for trace gases, with the deposition

167 velocity being determined by three categories of resistance: aerodynamic, quasi-laminar sublayer, and surface

168 resistance, encompassing soil and vegetation absorption. The latter is inclusive of both stomatal and nonstomatal

169 absorption. The dry deposition module, taken from the CLM4 surface scheme, covers 29 gas-phase species and

170 comprises 11 types of land cover. To enhance the accuracy of the daily variation in dry deposition simulation,

171 both stomatal and nonstomatal resistances are accounted for in the dry deposition scheme. The calculation of all

172 deposition resistances is performed within the CLM land surface model (Wesely, 1989). Wet deposition uses the

173 MOZART global model's wet deposition parameterization scheme (Emmons et al., 2010; Horowitz et al., 2003),

174 including 26 gas-phase species in CBM-Z, and the wet deposition amount is based on the simulated precipita-

175 tion.

176 **2.3 Descriptions of the YIBs model**

177   The YIBs model, pioneered by Yale University, integrates plant physiological mechanisms to simulate how

178 photosynthesis, respiration, and other physiological processes respond to environmental drivers such as radia-

179 tion, temperature, and moisture. Moreover, YIBs simulates the carbon cycle both regionally and globally (Yue

180 and Unger, 2015). For example, its simulation of terrestrial carbon flux closely matches ground flux observa-

181 tions and satellite-derived data in diverse geographical areas such as the United States and China (Yue and

182 Unger, 2017; Yue et al., 2017).

183 **2.3.1 The main processes in YIBs**

184   In the YIBs model, eight distinct Plant Functional Types (PFTs) are incorporated, encompassing evergreen

185 coniferous forest, evergreen broad-leaved forest, deciduous broad-leaved forest, shrub forest, tundra, C3 grass-

186 land, C4 grasslands, and crops. The model employs the Michaelis–Menten enzyme-kinetics scheme for simulat-

187 ing plant photosynthesis (Farquhar et al., 1980), and the total photosynthesis (A_{tot}) of leaves is affected by Ru-

188 bisco enzyme activity (J_c), electron transfer rate (J_e), and photosynthetic product (triose phosphate) transport

189 capacity (J_S) limitation.

2.3.2 Canopy Radiation Scheme

191   A multilayer canopy radiation transmission scheme is adopted in YIBs for canopy radiation transmission

192 (Spitters et al., 1986), consisting of a radiation transfer model based on the total leaf area index, extinction coef-

193 ficient, and vegetation height. The entire vegetation canopy is usually divided into 2 to 16 layers, and the spe-

194 cific number of layers can be automatically adjusted according to the height of the canopy.

2.3.3 Biogenic Volatile Organic Compound Emission Scheme

196   Differently from the traditional MEGAN scheme, the YIBs model applies a biogenic volatile organic com-

197 pound (BVOC) emission scheme on a leaf scale, which is better suited to describe the photosynthesis process in

198 vegetation (Guenther et al., 1995). This introduces an effect of plant photosynthesis on BVOC emissions which

199 is more closely related to the real physiological process of vegetation. BVOC emissions from leaves to the can-

200 opy are integrated to obtain total canopy emissions. The intensity of leaf BVOC emission depends on the rate of

201 photosynthesis J_e under electron transfer rate limitation, leaf surface temperature, and intracellular CO_2 con-

202 centration (Yue and Unger, 2015):

$$I = J_e \cdot \beta \cdot \kappa \cdot \tau \cdot \varepsilon \qquad (1)$$

204 where I is the intensity of leaf BVOC emission in units of $\mu mol\ m^{-2}[leaf]\ s^{-1}$, J_e is the electron

205 transport-limited photosynthesis rate, the calculation formula is as follows:

$$J_e = a_{leaf} \cdot PAR \cdot \alpha_{qe} \cdot \frac{C_i - \Gamma^*}{C_i - 2\Gamma^*}, \qquad (2)$$

207 where α_{leaf} is the leaf-specific light absorbance, PAR is photosynthetically active radiation, α_{qe} is the intrin-

208 sic quantum efficiency for photosynthetic CO_2 uptake in the chlorophyll reaction system. C_i is the internal leaf

209 CO_2 concentration. Γ^* is the CO_2 concentration compensation point in the absence of non-photorespiratory

210 respiration (Collatz et al., 1991).

211 β is the coefficient for converting electron transfer flux into BVOC emissions (Niinemets et al., 1999;

212 Pacifico et al., 2011):

$$\beta = \frac{C_i - \Gamma^*}{6(4.67C_i + 9.33\Gamma^*)}, \qquad (3)$$

214 where κ is related to the internal leaf CO_2 concentration:

215
$$\kappa = \frac{C_{i\_standard}}{C_i}, \qquad (4)$$

216 where $C_{i\_standard}$ is the internal leaf CO_2 concentration under standard conditions (when atmospheric CO_2 is

217 370 ppm). The τ term reflects the response of BVOC emission intensity to temperature:

218
$$\tau = \exp[0.1(T - T_{ref})], \qquad (5)$$

219 where T is the blade surface temperature, T_{ref} is the standard temperature (30 °C). When the blade temperature

220 is 40 °C, the BVOC emission intensity is maximum. As the temperature further rises, the BVOC emission grad-

221 ually weakens. In reality, such high temperatures are relatively rare and may only occur under extremely dry

222 climate conditions.

223 **2.3.4 Ozone Damage Protocol**

224   When tropospheric ozone enters plants through stomata, it can directly damage plant cell tissues, thereby

225 slowing the photosynthesis rate and further weakening the carbon sequestration capacity of vegetation. The

226 YIBs model incorporates the semi-mechanistic parameterization scheme to delineate ozone's effect on plants

227 (Sitch et al., 2007):

228
$$A = A_{tot} \cdot F \qquad (6)$$

229 where A is photosynthesis minus the influence of ozone, A_{tot} is the total photosynthesis of leaves, F is the

230 proportion of photosynthesis minus the influence of ozone, which depends on the ozone flux from the stomata

231 into the vegetation that exceeds the threshold.

232
$$F = 1 - a \cdot \max[(F_{ozn} - F_{ozncrit}), 0] \qquad (7)$$

233 where a is the sensitivity parameter of vegetation to ozone obtained based on observation data. $F_{ozncrit}$ repre-

234 sents the threshold corresponding to the damage caused by ozone to vegetation, F_{ozn} represents the flux of

235 ozone entering the page through the stomata:

236
$$F_{ozn} = \frac{[O_3]}{r_b + \frac{\kappa_{O3}}{r_s}}, \qquad (8)$$

237 where $[O_3]$ is the ozone concentration at the top of the canopy, r_b is the boundary layer resistance, κ_{O3} is the

238 ratio of O_3 leaf resistance to water vapor blade resistance, r_s is the stomatal resistance considering the influence

239 of ozone:

240
$$r_s = g_s \cdot F \qquad (9)$$

241 g_s is the leaf conductance without O_3 effects. The set of equations (7), (8) and (9) yields a quadratic term in F

242 that can be solved analytically.

243 **2.4 Descriptions of the RegCM-Chem-YIBs model**

244 **2.4.1 Coupling between RegCM-Chem and YIBs**

245   The integrated RegCM-Chem-YIBs model, an enhancement to the original RegCM-Chem, introduces CO_2

246 as an atmospheric constituent, incorporating its source-sink dynamics, transport, and diffusion processes. At-

247 mospheric CO_2 concentration is primarily influenced by atmosphere-ocean CO_2 exchange flux, biomass com-

248 bustion emissions, fossil fuel emissions, and terrestrial ecosystem CO_2 flux. The model prescribes fossil fuel

249 emissions, biomass combustion emissions, and atmosphere-ocean CO_2 fluxes, while the terrestrial ecosystem

250 CO_2 fluxes are computed in real time via the coupled YIBs terrestrial ecosystem model.

251   Within the coupled model system, meteorological variables (including temperature, humidity, precipitation,

252 radiation, etc.) and atmospheric pollutant concentrations (O_3 and $PM_{2.5}$) generated by RegCM-Chem are incor-

253 porated into the YIBs model every six-minute intervals. This integration step is to be consistent with the integra-

254 tion time step of the chemistry module, thus maintaining synchronization between modules. Considering the

255 complexity of chemical reactions and ecological processes, dynamic adjustments at short intervals enable the

256 model to better capture transient interactions between ecology and the atmosphere. The choice of this adjust-

257 ment frequency balances the representation of actual processes with computational efficiency, ensuring that

258 simulation results are both accurate and efficient. YIBs then simulates vegetation physiological processes such

259 as photosynthesis and respiration, computing land surface parameters including CO_2 flux, BVOC, and stomatal

260 conductance. These outputs from the YIBs are subsequently integrated back into the RegCM-Chem model every

261 six-minute intervals, the intricacies of this integration process lead to significant changes in various environ-

262 mental parameters. The major direct changes, prominently influencing the model's behavior, arise from altera-

263 tions in CO_2 concentration. These changes are directly attributed to intricate physiological processes within the

264 vegetation, including photosynthesis and respiration. The fluxes of CO_2 through these biological processes play

265 a pivotal role in shaping the atmospheric composition. On the indirect front, the integration of YIBs outputs in-

266 duces intricate variations in $PM_{2.5}$ and O_3 concentrations. These indirect changes are primarily orchestrated by

267 shifts in BVOC emissions. The dynamic nature of these emissions contributes to the complexity of atmospheric

268 chemistry, influencing the levels of $PM_{2.5}$ and O_3. Simultaneously, the integration process plays a crucial role in

269 shaping the temporal variations of atmospheric temperature, humidity, and circulation. These changes over time

are intricately linked to variations in land surface parameters. The interplay of these variables illustrates the dynamic feedback loops between climate, chemical composition, and ecological processes within the integrated model system. ~~modulating atmospheric composition (CO_2, O_3, and $PM_{2.5}$) and atmospheric variables (atmospheric temperature, humidity, and circulation), thereby describing the interplay of climate, chemical, and ecological processes.~~

2.4.2 Model input data

The input data of RegCM-Chem-YIBs mainly includes four categories: surface data, initial boundary data, anthropogenic emission data and CO_2 surface flux data, which are detailed below.

(1) Surface data include surface vegetation cover type, terrain, and leaf area index. Land cover type information is obtained from the MODIS and AVHRR satellites, employing the classification scheme suggested by Lawrence and Chase (Lawrence and Chase, 2007), which uses MODIS data to preliminarily distinguish forest, grassland, bare soil, etc., and combine this with AVHRR data to make a detailed forest classification. The dataset contains a total of 16 different vegetation functional types. To align with the classification conventions of the YIBs model, the original 16 vegetation functional types were converted into the corresponding 8 types recognized by the YIBs model. The results are shown in Figure S1.

(2) Initial and boundary data include initial and boundary conditions of meteorological variables and atmospheric chemical composition. Here we use ERA-Interim reanalysis meteorological data, a product from the European Center for Medium-Range Weather Forecasts (ECMWF) created through four-dimensional variational assimilation. The data is on 37 vertical levels, with a horizontal resolution of 0.125°×0.125°, and time resolution of 6 hours. Data for Sea Surface Temperature (SST) is provided by the weekly averaged Optimum Interpolation SST product (OI_WK) of the National Oceanic and Atmospheric Administration (NOAA) (Reynolds et al., 2002). The initial and boundary conditions of atmospheric chemical components (e.g. O_3), come from simulations carried out with the global chemistry model MOZART (Emmons et al., 2010; Horowitz et al., 2003). In addition, the initial and boundary conditions for CO_2 species come from the CarbonTracker global carbon assimilation system (Peters et al., 2007) developed by NOAA Earth System Research Laboratory ESRL (Earth System Research Laboratory), which uses the ensemble Kalman filter algorithm to assimilate ESRL greenhouse gas observations and CO_2 observation data provided by the network of collaborating institutions worldwide. The assimilated data includes not only conventional fixed-site observations but also mobile monitoring data such as

298 aircraft and ships. Since 2007, yearly updated carbon assimilation products are provided by CarbonTracker, de-

299 livering global CO_2 three-dimensional concentration data products every three hours. In this study, we utilized

300 the CT2019 product, updated in 2019, spanning a period from January 1, 2000 to March 29, 2019.

301 (3) Anthropogenic emission data include precursors of ozone and particulate matter such as NOx, VOC,

302 BC, OC, etc. The MIX Asian anthropogenic emission inventory developed by the Tsinghua University is used

303 (Li et al., 2017b), which integrates the results of the emission inventories of various regions in Asia. The emis-

304 sions in China come from China's multi-scale emission inventory MEIC (Multi-resolution Emission Inventory

305 for China) and the high-resolution NH_3 emission inventory developed by Peking University. The anthropogenic

306 emissions in India come from the Indian local emission inventory developed by ANL (Argonne National Labor-

307 atory), while the anthropogenic emissions in South Korea come from the CAPSS (The Korean local emission

308 inventory developed by the Policy Support System), and the man-made emissions in other regions are provided

309 by the REAS (Regional Emission inventory in Asia) emission inventory version 2.1. The anthropogenic emis-

310 sions of major pollutants in the simulated area are shown in Figure S2.

311 (4) Data pertaining to fossil fuel CO_2 emissions are sourced from the MIX Asian anthropogenic emission

312 inventory with a monthly time resolution. CO_2 emissions resulting from biomass burning are derived from the

313 FINN (Fire Inventory from NCAR) inventory (Wiedinmyer et al., 2011) developed by the National Center for

314 Atmospheric Research. The FINN inventory has a daily time resolution. The model's ocean-atmosphere CO_2

315 exchange flux is obtained from the carbon flux product of the CarbonTracker assimilation system, constructed

316 with the global atmospheric transport model TM5 and assimilating CO_2 observation data via an ensemble Kal-

317 man filter algorithm. This provides global $1° \times 1°$ resolution CO_2 exchange flux data between the ocean and the

318 atmosphere updated every three hours. The emissions are detailed in Figure S3.

319 **3 Model Application**

320 **3.1 Model setup**

321 To evaluate the performance of RegCM-Chem-YIBs we carried out a one-year simulation starting from

322 December 1st, 2015, through December 31st, 2016. The initial month is used as spin-up period, and thus it is not

323 included in the analysis. The simulation domain is centered at 36°N, 107°E, and covers a considerable part of

324 East Asia, including China, Japan, the Korean Peninsula, and Mongolia, along with significant parts of India and

Southeast Asia (Figure S4). The horizontal grid spacing is 30 km and we use 14 levels in the vertical, reaching up to 50 hPa. Section 2.4.2 provides a comprehensive description of the model input data.

3.2 Climate simulations in East Asian

Given the importance of the climate for the East Asia region, we first present an assessment of the simulation for the climate 2016 by comparison with the ERA-Interim data. The simulated temperature, specific humidity, and wind fields at varying altitudes and seasons compared well with the reanalyzed data (Figure S5~ Figure S9), especially temperature and specific humidity, while a tendency to overestimate wind speed is observed at the near surface and 850 hPa levels. The fields at 500 hPa show very close agreement with reanalysis data, indicating a strong mid-atmosphere forcing by the boundary conditions, while the simulated circulation patterns near the surface and at 850 hPa in summer tend to deviate more from the driving reanalysis. The simulated circulation patterns in the other seasons are basically consistent with the reanalysis data.

We first calculated the daily average of the meteorological variables, such as temperature, wind speed, and specific humidity, from the model simulation and reanalysis data, respectively. Then we calculate the corresponding statistical indicator correlation coefficient (R), mean deviation (MB), and root mean square error (RMSE) based on the daily averages. Table 1 reports a number of statistical metrics of comparison between simulated and reanalysis meteorological variables at different heights. Correlation coefficients (R) range from 0.95 to 0.98 for temperature, 0.71 to 0.97 for longitudinal wind, 0.81 to 0.92 for latitudinal wind, and 0.91-0.92 for specific humidity, indicating a general good consistency between model and driving data, in line with previous studies (Zhuang et al., 2018; Zhou et al., 2014; Wang et al., 2010).

Table 1. Statistical indicators for comparison between model simulation results and reanalysis data

Heights	Statistical index	Air Temperature(K)	Longitudinal wind (m/s)	Latitudinal wind (m/s)	Specific humidity (kg kg^{-1})
	R	0.98	0.97	0.92	0.91
500 hpa	MB	0.15	0.35	-0.03	0.00015
	RMSE	0.93	0.75	0.51	0.00019
	R	0.96	0.77	0.85	0.94
850 hpa	MB	-0.98	0.38	0.15	-0.00066
	RMSE	1.1	1.08	0.59	0.00077

Near sur-face	R	0.95	0.71	0.81	0.92
	MB	-1.21	0.33	0.23	-0.00098
	RMSE	1.35	0.59	0.54	0.00112

(Correlation coefficients (R), mean biases (MB), and root mean square error (RMSE))

The magnitude of surface radiation flux directly determines the rates of photosynthesis in vegetation. For verification purposes, model surface solar fluxes were compared with data on solar energy at the surface retrieved from the Clouds and the Earth's Radiant Energy System (CERES) satellite, which has a $1° \times 1°$ horizontal and monthly temporal resolution. Figure S10 shows the simulated surface net shortwave radiation in different seasons and comparison with observational data. The model tends to overestimate surface net shortwave radiation in spring and winter over India and summer over North China (Yin et al., 2014). Overall, the simulated surface net shortwave radiation agrees well with the CERES satellite retrieval results, capturing the spatial distribution and seasonal fluctuation patterns of surface shortwave radiation. The simulation findings from our study are consistent with earlier research regarding surface net shortwave radiation (Han et al., 2016).

In conclusion, RegCM-Chem-YIBs demonstrates a good performance in simulating the climatological features of the East Asia atmospheric circulations, effectively reproducing the spatial distribution and seasonal variations of temperature, specific humidity, and radiation.

3.3 Simulations of $PM_{2.5}$, O_3 and CO_2

In this section, we compare simulated $PM_{2.5}$ and O_3 concentrations against observational data from 366 stations provided by the China National Environmental Monitoring Center. The geographical distribution of the simulated annual mean near-surface daily $PM_{2.5}$ and maximum daily 8-hour average (MDA8) O_3 concentration, along with the observed values, are shown in Figure 2. Supplementary Figure S11 then compares in a scat-ter-plot format the observation and simulation results. Both figures demonstrate that the model reproduces the spatial distribution patterns of $PM_{2.5}$ and O_3, with a significant agreement between modeled and measured values across all stations. The statistical indicators of simulated and measured surface $PM_{2.5}$ and O_3 levels are shown in Table S1, showing a correlation between simulation and observations of O_3 and $PM_{2.5}$ of 0.74 and 0.65, respectively. The simulated O_3 concentrations are generally lower than observed in the Fenwei Plain of China, a discrepancy possibly attributable to uncertainties in the emission inventory for this region. In summary, the RegCM-Chem-YIBs model demonstrates a good ability to capture the spatial distribution of observed

370 near-surface ozone and particulate matter, especially in highly polluted areas.
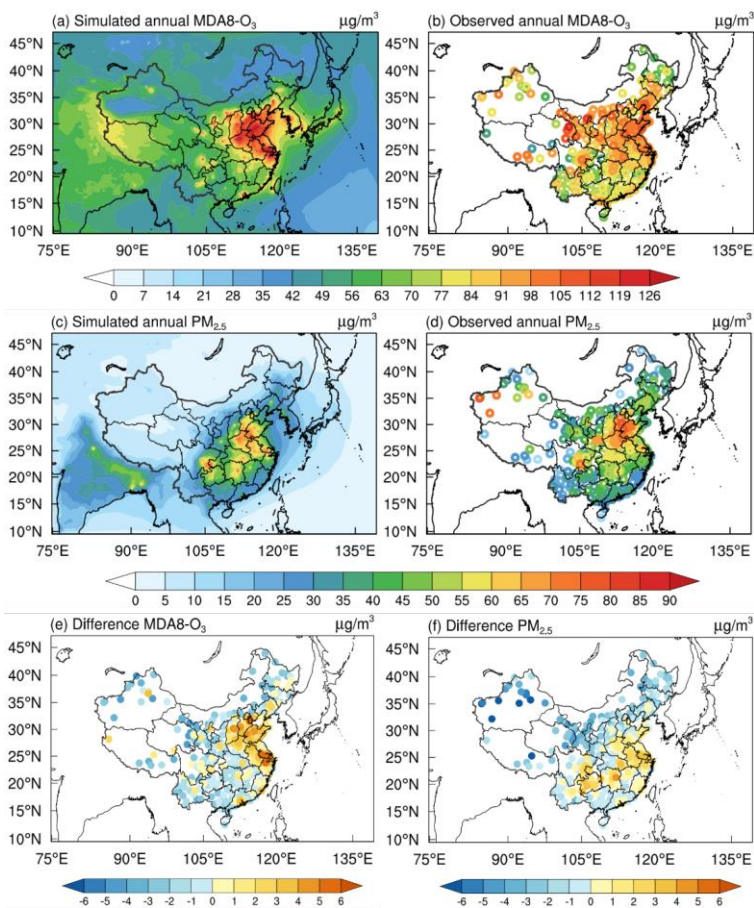
Figure 2. Simulation and observation comparison of (a, b) O_3 and (c, d) $PM_{2.5}$ and their differences (e, f) in China. The differences are simulation minus observation. The colored circles in the figure represent station observations. Units: μg m^{-3}.

Measured and calculated monthly mean CO_2 concentrations at six observation stations in East Asia from the World data Center for Greenhouse Gases are shown in Figure 3. Information on the six sites is listed in Table 2. The simulated CO_2 concentration agrees well with observations, with correlation coefficients ranging from 0.89 to 0.97. However, in urban and coastal areas, the model performance deteriorates likely due to local emission fluctuations and errors in biogenic fluxes. Nevertheless, the model overall captures the seasonal variations in CO_2 concentrations (Figure 3). This result likely stems from the complex relationship between biogenic and

fossil fuel emissions, which are known contributors to observed seasonal CO_2 patterns (Kou et al., 2015). A high CO_2 mixing ratio (412.3 ppm) is observed at the TAP site, which is associated with strong local emissions. Further analysis into the specific sources contributing to elevated CO_2 levels would provide valuable insights into localized patterns of emissions and their effects on regional carbon cycle processes. The model's ability to reproduce the geographical and seasonal CO_2 patterns serves as an illustration of its ability to capture the main processes driving CO_2 dynamics. In summary, while discrepancies in urban or coastal areas highlight the challenges associated with capturing localized CO_2 dynamics, the model's overall performance and ability to reproduce geographical and seasonal CO_2 patterns demonstrates its usefulness in studying CO_2 dynamics at a regional scale.

Table 2. Information on six CO_2 stations in East Asia and statistical indicators of observed and modeled CO_2.

Sites	Latitude	Longitude	Elevation	Observations (ppm)	Simulations (ppm)	R	RMSE
WLG	36.29	100.90	3810	404.3	402.9	0.94	1.75
TAP	36.72	126.12	20	412.3	414.8	0.97	2.70
UUM	44.45	111.08	992	405.7	403.7	0.96	2.66
LLN	23.46	120.86	2867	406.0	407.2	0.93	1.63
YON	24.47	123.02	30	407.1	407.4	0.89	2.80
HK	22.31	114.17	65	407.9	409.7	0.92	15.67

(Correlation coefficients (R) and root mean square error (RMSE))
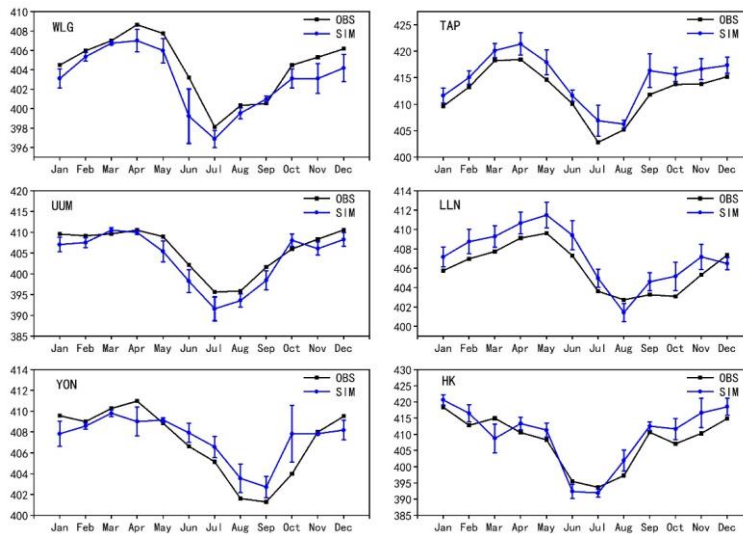
Figure 3. Modeled (blue) and observed (black) monthly mean CO_2 concentrations validated at six sites in East Asia. Units: ppm.

The limitations of ground-based CO_2 observation stations, particularly their sparse spatial distribution, pose challenges in obtaining high-resolution CO_2 data. To offset this limitation, data assimilation methods have been implemented to ensure a coherent global distribution of atmospheric CO_2, effectively filling the void left by sparse ground-based observations. Here we utilize the Carbon Tracker global carbon assimilation system developed by the NOAA Earth System Research Laboratory (ESRL) to validate the simulated CO_2 concentrations (Peters et al., 2007). This comparison for the year 2016 is shown in Figure 4. The simulated CO_2 concentrations tend to be lower than observed in Northeastern India and Northeastern China, while they show a better agreement with observations in other regions. These discrepancies can be traced back to factors such as the underestimation of localized CO_2 emissions along with the effects of complex topography and circulation patterns. However, the closer agreement in other regions suggests that the model effectively captures the primary processes driving CO_2 concentrations.

Seasonal variations in the spatial distribution of CO_2 concentrations for 2016 are illustrated in supplementary Figure S12. The simulations show marked seasonal variations, with elevated concentrations in spring, autumn, and lower values during summer. In northern regions, including Russia, Mongolia, and Northeast China, the lowest near-surface CO_2 concentrations occur in summer. This pattern can be attributed to the enhanced

photosynthetic activity of terrestrial vegetation in summer, leading to enhanced atmospheric CO_2 sequestration. Conversely, winter months are characterized by lower solar radiation fluxes and reduced vegetation photosynthesis, resulting in relatively higher CO_2 concentrations. In specific regions, notably the eastern coastal zones of China and South Korea, the seasonal pattern of CO_2 concentration is reduced, likely because of the high levels of urbanization, dense population, and intense anthropogenic emissions in these areas. In contrast, regions such as Yunnan, the southern side of the Qinghai-Tibet Plateau, and Southeast Asia exhibit consistently low CO_2 concentrations during summer because of significant vegetation sinks in these densely vegetated areas. An increase in CO_2 concentrations can be observed over these regions during spring due to local forest fires and straw-burning processes, which release substantial amounts of CO_2 into the atmosphere (Chuang et al., 2014).
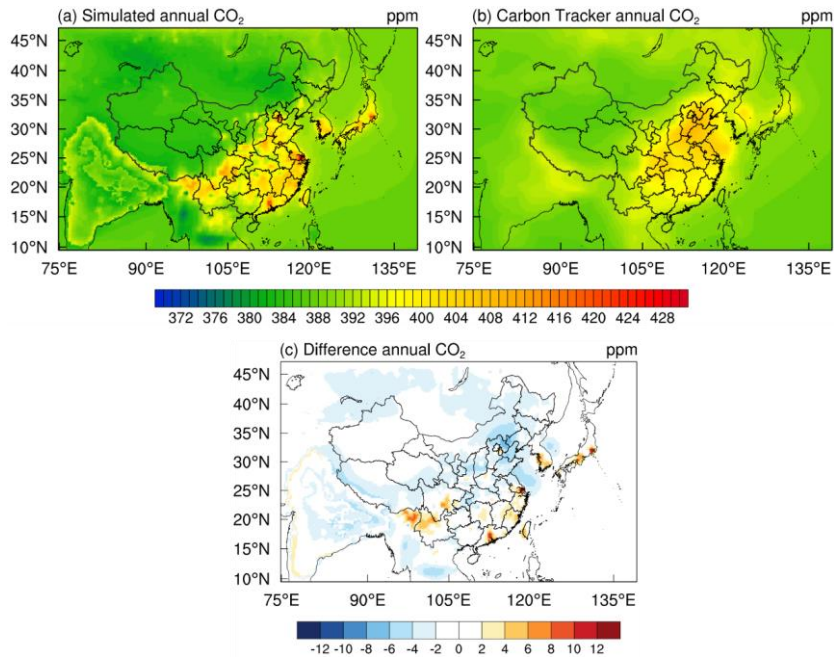
Figure 4. Evaluation of simulated CO_2 (a) using Carbon Tracker products (b) and their difference (c) in 2016. The differences are simulation minus observation. Units: ppm.

3.4 Simulations of carbon fluxes in terrestrial systems

Our assessment of GPP and NPP uses the MOD17A3 Collection 6, a global product originating from MODIS satellite observations. GPP data include 8-day values with a resolution of 500 meters, as produced in

425 MOD17A2H Version 6 based on radiation use efficiency theory. Such data can be used as input to computations

426 of terrestrial carbon and energy flows, water cycling processes, and vegetation biogeochemistry. Moreover, the

427 MOD17A3H Version 6 product provides information on annual NPP, also on a resolution of 500 meters. All

428 8-day Net Photosynthesis (PSN) products (MOD17A2H) from a particular year are combined to derive annual

429 NPP values (He et al., 2018; Madani et al., 2014; Running, 2012).

430 Figure 5 (a, b, e) shows the geographical distribution of the mean GPP in 2016 from the model simulations

431 and MODIS products. RegCM-Chem-YIBs effectively captures the observed spatial GPP features, with high

432 values mostly over Southwest, Central, and Southeastern China, areas characterized by deciduous broad-leaf

433 and evergreen coniferous forests (Figure S1). The annual average GPP simulated by RegCM-Chem-YIBs is

434 higher than observed over   Southwest and Central China by 6.8% and 12.7%, respectively. The annual average

435 simulated GPP over China is 6.18 Pg C yr^{-1}, which is about 7.56% higher than the GPP in MODIS.

436 Figure 6 (a) and Table S2 show the scatter plots of the simulated annual average GPP on each model grid

437 point compared with MODIS. A correlation coefficient of 0.91 and root mean square error of 0.4 kg C m^{-2} yr^{-1} is

438 found,   reflecting an overall good simulation by the model. Compared with the results obtained from the global

439 model NASA ModelE2–YIBs (Yue and Unger, 2017), the GPP value estimated here compares better with the

440 MODIS product, which may also be attributed to the higher spatial resolution of the regional system. Moreover,

441 our GPP results are also in line with earlier findings, such as from Li (Li et al., 2013b) who estimated an annual

442 average GPP over China of 6.04 Pg C yr^{-1} based on the light energy utilization model EC-LUE.

443 Figure 5 (c, d, f) shows the spatial distribution of mean NPP for both the simulations and MODIS

444 products in 2016. NPP, similarly to GPP, exhibits a gradual reduction from southeast to northwest China. The

445 scatter plot comparing the simulated and MODIS annual average NPP across the model grid is illustrated in

446 Figure 6 (b). According to Table S2, a correlation coefficient of 0.87 is found between the simulated and

447 MODIS NPP, with a root mean square error of 0.22 kg C m^{-2} yr^{-1}. Notably, the simulated NPP shows a distinct

448 underestimation over regions with higher NPP values. Compared with the MODIS NPP data products, the

449 annual average NPP simulated for the entire China region in 2016 is overestimated by approximately 8.64%,

450 mostly because of the model overestimate in Central China (16.6%).

451 Part of the reason for this result is the relatively simple treatment of the nitrogen deposition process in YIBs

452 (Yue and Unger, 2015). On the other hand, some studies have noted that due to the limitations of driving data

453 and algorithm parameters, the MODIS NPP products have some problems in China (Li et al., 2013b).

454 Furthermore, the NPP value estimated by the model over China is 3.21 Pg C yr^{-1}, in line with the mean value

455 (2.92 ± 0.12 Pg C yr^{-1}) found in previous 37 studies (Wang et al., 2017).
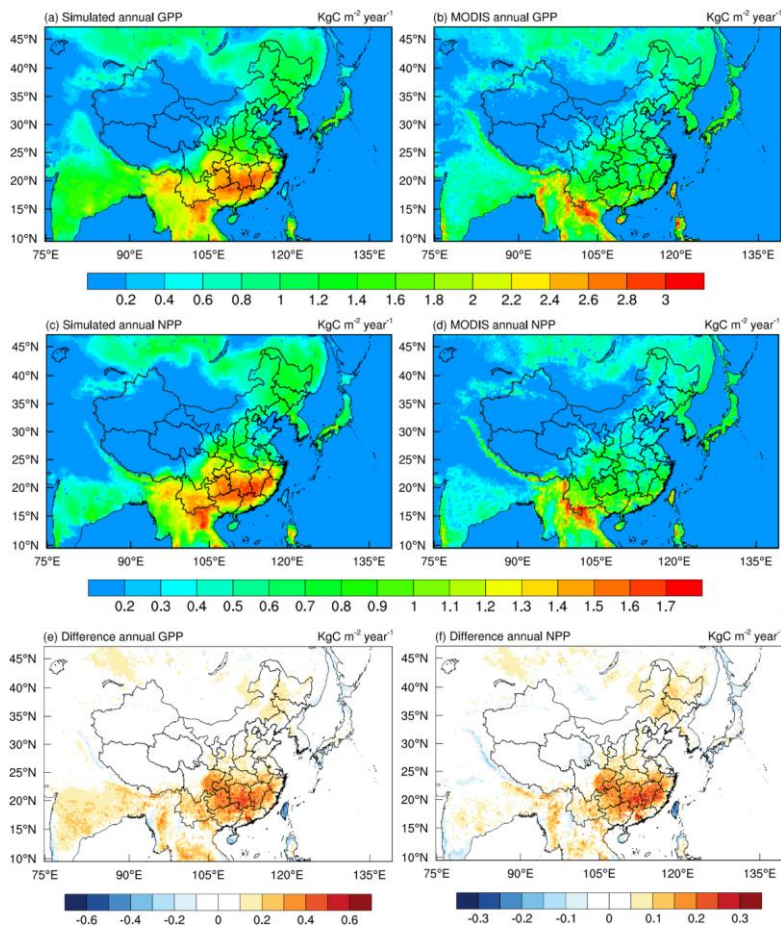
456

457 **Figure 5.** Spatial distribution of modeled (a, c) and MODIS (b, d), annual mean GPP (a, b) and NPP (c, d), and

458 their differences (e, f). The differences are simulation minus observation. Units: kg C m^{-2} year^{-1}.

459
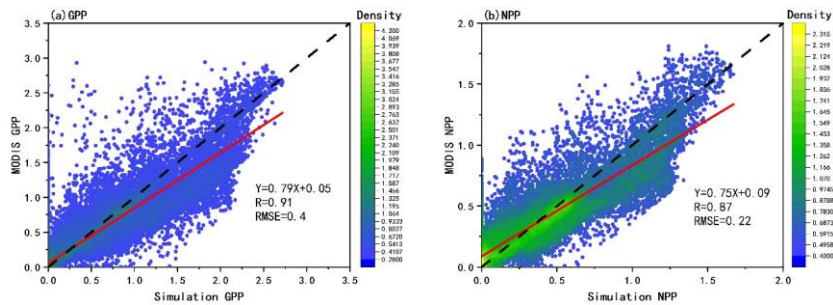
Figure 6. Density scatter plots of (a) GPP and (b) NPP for model simulations and inversion-based products for

461   2016. Units: kg C m^{-2} year^{-1}.

Figure 7 and Figure 8 illustrate the seasonal fluctuations in GPP and NPP, as simulated for 2016 in East

Asia. Both GPP and NPP present pronounced seasonal variations, with negligible values during winter, and a

strong peak in summer.   The winter minimum is attributable to limiting environmental factors such as reduced

solar radiation, lower temperatures, and suppressed photosynthetic activity by vegetation. Conversely, summer

shows the highest GPP and NPP values due to extended daylight hours, increased solar radiation, and

temperatures facilitating increased photosynthetic activity and vegetation metabolism.

468
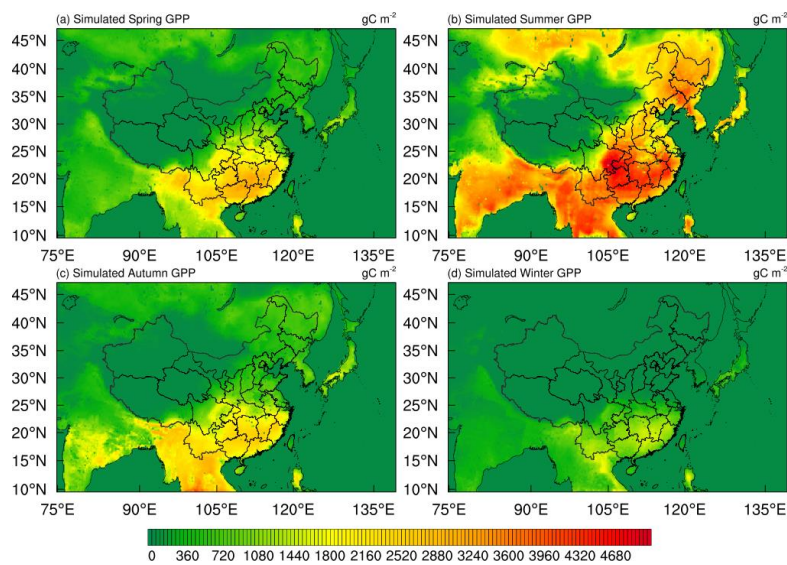
Figure 7. Spatial distribution of GPP simulated by model of spring(a), summer(b), autumn(c) and winter(d) in
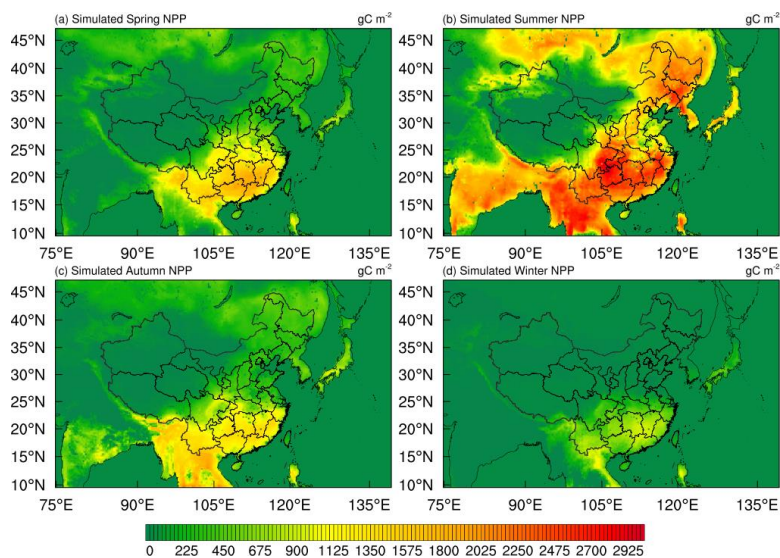
470   2016. Units: g C m^{-2}

Figure 8. Spatial distribution of NPP simulated by model of spring(a), summer(b), autumn(c) and winter(d) in 2016. Units: g C m^{-2}

3.5 Simulations of other carbon-bearing species

The analysis of additional carbonaceous compounds such as BC, OC and carbon monoxide (CO), is crucial due to their considerable influence on climate and the carbon cycle. The spatial distribution of simulated BC for each season of 2016 is shown in Figure S13. BC concentrations are mainly centered in North China, Central China, the Sichuan Basin, Chongqing, and Northeast India, regions with a higher concentration of industrial and residential emission sources. BC displays a marked seasonal variation, with elevated levels in winter, possibly attributed to residential heating, more stagnant conditions, and reduced removal by precipitation.

Figure S14 then shows the spatial corresponding distribution of seasonal OC, which is also higher over North China, Central China, Sichuan and Chongqing, and Northeast India. Finally, Figure S15 reports the annual mean near-surface CO concentrations for observations and simulation data across the monitoring sites in China. While simulated CO concentrations agree well spatially with observations, the simulations produce higher values than observed in Central China, likely linked to uncertainties in emission inventories. Figure S16 presents the seasonal spatial distributions of CO, with simulated high values mostly localized in Sichuan-Chongqing and Central China, and a peak in winter.

4 Conclusions

Regional climate-chemical coupled models can be used to study the characteristics of regional-scale climate and pollutants, and is an important means to investigate the behavior of atmospheric pollutants and their radiative climate effects. However, current coupled regional climate models describe the physiological process of terrestrial vegetation relatively simply and do not consider the interaction between atmospheric pollutants (such as $PM_{2.5}$ and O_3) and CO_2, as well as their impacts on terrestrial ecosystems.

To overcome this problem, in this work we coupled the YIBs biogeochemical model to the RegCM-CHEM regional climate-chemistry model, and tested this coupled modeling system over a domain covering East Asia at a 30 km horizontal grid spacing for the year 2016. The model output was validated against reanalysis data, observational data, and satellite remote sensing data, both for the atmosphere and the carbon cycle.

Our simulations show that the coupled RegCM-Chem-YIBs system can effectively reproduce the spatio-temporal distribution of meteorological variables, atmospheric composition ($PM_{2.5}$, O_3, and CO_2) and terrestrial carbon fluxes (GPP and NPP). Comparisons of the simulated temperature, longitudinal wind, latitudinal wind, and specific humidity for different seasons with the driving ERA-Interim reanalysis data showed correlation coefficients of 0.95-0.98, 0.71-0.97, 0.81-0.92, and 0.91-0.92, respectively. The correlation coefficients between observed and simulated O_3 and $PM_{2.5}$ levels in China were 0.74 and 0.65, respectively, while the corresponding correlations for CO_2 were in the range of 0.89 to 0.97. Comparison of the ecological parameters GPP and NPP simulated in East Asia with the observed data showed correlation coefficients of 0.91 and 0.87, respectively. In addition, in all cases, the seasonal variation of the different variables was captured by the model. Therefore, we conclude that, overall, the RegCM-Chem-YIBs model demonstrates a good performance in simulating the spatio-temporal distribution characteristics of regional meteorological characteristics, atmospheric composition, and ecological parameters over East Asia.

In the future, we will continue to improve RegCM-Chem-YIBs in the following aspects. First, we will investigate the impact of CO_2 and O_3 inhomogeneity on radiation calculations by integrating temporally and spatially varying concentrations derived from YIBs and Chem into the RegCM radiation module. This will enable additional accurate computation of longwave radiation flux, improving the representation of the regional radiation balance. Second, we intend to assimilate a module representing various chemical transformations happening on the surfaces of aerosol particles. Finally, we will include the wet removal process of O_3. These advancements will contribute to the refinement of RegCM-Chem-YIBs, enhancing our ability to investigate the interactions

between regional atmosphere, carbon cycle, and vegetation processes.

Code and data availability

The RegCM-Chem source code can be obtained from https://github.com/ICTP/RegCM (last access: 10 July 2023). The YIBs model code is available at https://github.com/YIBS01/YIBs_site (last access: 10 July 2023). The input data and source code for RegCM-Chem-YIBs have been archived on Zenodo at https://doi.org/10.5281/zenodo.8186164 (Xie and Wang, 2023). The CarbonTracker data are provided at (https://gml.noaa.gov/ccgg/carbontracker/). The CERES surface radiation data are available at (https://ceres.larc.nasa.gov/). WDCGG data are available at (https://gaw.kishou.go.jp/). CNEMC data are provided at (http://www.cnemc.cn/). MODIS data are available at (https://ladsweb.modaps.eosdis.nasa.gov/).

Author contributions

TW led the development of RegCM-Chem-YIBs with significant contributions from NX and XX. NX performed the evaluation. NX, TW drafted the manuscript and all authors contributed to review and editing of the manuscript.

Competing interests

The corresponding author has stated that all the authors have no conflicts of interest.

Disclaimer

Publisher's note: Copernicus Publications remains neutral about jurisdictional claims in published maps and institutional affiliations.

Acknowledgments

This work was supported by the National Natural Science Foundation of China (42077192), the National Key Basic Research & Development Program of China (2020YFA0607802), the Creative talent exchange program for foreign experts in the Belt and Road countries, and the Emory University-Nanjing University Collaborative Research Grant.

References

Ahlstrom, A., Raupach, M. R., Schurgers, G., Smith, B., Arneth, A., Jung, M., Reichstein, M., Canadell, J. G., *et al.*: The dominant role of semi-arid ecosystems in the trend and variability of the land CO2 sink, Science, 348, 895-899, https://doi.org/10.1126/science.aaa1668, 2015.

Ainsworth, E. A., Yendrek, C. R., Sitch, S., Collins, W. J., and Emberson, L. D.: The Effects of Tropospheric Ozone on Net Primary Productivity and Implications for Climate Change, Annu. Rev. Plant Biol., 63, 637-661, https://doi.org/10.1146/annurev-arplant-042110-103829, 2012.

Artale, V., Calmanti, S., Carillo, A., Dell'Aquila, A., Herrmann, M., Pisacane, G., Ruti, P. M., Sannino, G., *et al.*: An atmosphere-ocean regional climate model for the Mediterranean area: assessment of a present climate simulation, Clim. Dyn., 35, 721-740, https://doi.org/10.1007/s00382-009-0691-8, 2010.

Baklanov, A., Molina, L. T., and Gauss, M.: Megacities, air quality and climate, Atmos. Environ., 126, 235-249, https://doi.org/10.1016/j.atmosenv.2015.11.059, 2016.

Chang, J. S., Brost, R. A., Isaksen, I. S. A., Madronich, S., Middleton, P., Stockwell, W. R., and Walcek, C. J.: A 3-DIMENSIONAL EULERIAN ACID DEPOSITION MODEL - PHYSICAL CONCEPTS AND FORMULATION, J. Geophys. Res.: Atmos., 92, 14681-14700, https://doi.org/10.1029/JD092iD12p14681, 1987.

Chuang, M. T., Lee, C. T., Chou, C. C. K., Lin, N. H., Sheu, G. R., Wang, J. L., Chang, S. C., Wang, S. H., *et al.*: Carbonaceous aerosols in the air masses transported from Indochina to Taiwan: Long-term observation at Mt. Lulin, Atmos. Environ., 89, 507-516, https://doi.org/10.1016/j.atmosenv.2013.11.066, 2014.

Chutia, L., Ojha, N., Girach, I. A., Sahu, L. K., Alvarado, L. M. A., Burrows, J. P., Pathak, B., and Bhuyan, P. K.: Distribution of volatile organic compounds over Indian subcontinent during winter: WRF-chem simulation versus observations, Environ. Pollut., 252, 256-269, https://doi.org/10.1016/j.envpol.2019.05.097, 2019.

Collatz, G. J., Ball, J. T., Grivet, C., and Berry, J. A.: Physio-logical and Environmental-Regulation of Stomatal Conductance, Photosynthesis and Transpiration – a Model That Includes a Laminar Boundary-Layer, Agric. For. Meteorol., 54, 107-136, https://doi.org/10.1016/0168-1923(91)90002-8, 1991.

Coppola, E., Poulton, M., Charles, E., Dustman, J., and Szidarovszky, F.: Application of Artificial Neural Networks to Complex Groundwater Management Problems, Nat. Resour. Res., 12, 303-320, https://doi.org/10.1023/B:NARR.0000007808.11860.7e, 2003.

Dickinson, R. E., Errico, R. M., Giorgi, F., and Bates, G. T.: A Regional Climate Model for the Western United-States, Clim. Change, 15, 383-422, https://doi.org/10.1007/BF00240465, 1989.

Dunne, J. P., Horowitz, L. W., Adcroft, A. J., Ginoux, P., Held, I. M., John, J. G., Krasting, J. P., Malyshev, S., *et al.*: The GFDL Earth System Model Version 4.1 (GFDL-ESM 4.1): Overall Coupled Model Description and Simulation Characteristics, J. Adv. Model. Earth Syst., 12, https://doi.org/ARTNe2019MS00201510.1029/2019MS002015, 2020.

Emmons, L. K., Walters, S., Hess, P. G., Lamarque, J. F., Pfister, G. G., Fillmore, D., Granier, C., Guenther, A., *et al.*: Description and evaluation of the Model for Ozone and Related chemical Tracers, version 4 (MOZART-4), Geosci. Model Dev., 3, 43-67, https://doi.org/10.5194/gmd-3-43-2010, 2010.

Farquhar, G. D., Caemmerer, S. V., and Berry, J. A.: A biochemical model of photosynthetic CO2 assimilation in leaves of C3 species, Planta, 149, 78-90, https://doi.org/10.1007/BF00386231, 1980.

Fiore, A. M., Naik, V., and Leibensperger, E. M.: Air Quality and Climate Connections, J. Air Waste Manage. Assoc., 65, 645-685, https://doi.org/10.1080/10962247.2015.1040526, 2015.

Fiore, A. M., Naik, V., Spracklen, D. V., Steiner, A., Unger, N., Prather, M., Bergmann, D., Cameron-Smith, P. J., *et al.*: Global air quality and climate, Chem. Soc. Rev., 41, 6663-6683, https://doi.org/10.1039/c2cs35095e,

583 2012.

584 Forkel, M., Carvalhais, N., Rodenbeck, C., Keeling, R., Heimann, M., Thonicke, K., Zaehle, S., and Reichstein,
585  M.: Enhanced seasonal CO2 exchange caused by amplified plant productivity in northern ecosystems,
586  Science, 351, 696-699, https://doi.org/10.1126/science.aac4971, 2016.

587 Gao, Y. M., Zhuang, B. L., Wang, T. J., Chen, H. M., Li, S., Wei, W., Lin, H. J., and Li, M. M.:
588  Climatic-Environmental Effects of Aerosols and Their Sensitivity to Aerosol Mixing States in East Asia in
589  Winter, Remote Sens., 14, https://doi.org/10.3390/rs14153539, 2022.

590 Gery, M. W., Whitten, G. Z., Killus, J. P., and Dodge, M. C.: A Photochemical Kinetics Mechanism for Urban
591  and Regional Scale Computer Modeling, J. Geophys. Res.: Atmos., 94, 12925-12956,
592  https://doi.org/10.1029/JD094iD10p12925, 1989.

593 Giorgi, F.: Simulation of Regional Climate Using a Limited Area Model Nested in a General-Circulation Model,
594  J. Clim., 3, 941-963, https://doi.org/10.1175/1520-0442(1990)003<0941:Sorcua>2.0.Co;2, 1990.

595 Giorgi, F. and Bates, G. T.: The Climatological Skill of a Regional Model over Complex Terrain, Mon. Weather
596  Rev., 117, 2325-2347, https://doi.org/10.1175/1520-0493(1989)117<2325:TCSOAR>2.0.CO;2, 1989.

597 Giorgi, F. and Mearns, L. O.: Introduction to special section: Regional climate modeling revisited, J. Geophys.
598  Res.: Atmos., 104, 6335-6352, https://doi.org/10.1029/98jd02072, 1999.

599 Giorgi, F., Marinucci, M. R., Bates, G. T., and Decanio, G.: DEVELOPMENT OF A 2ND-GENERATION
600  REGIONAL CLIMATE MODEL (REGCM2) .2. CONVECTIVE PROCESSES AND ASSIMILATION OF
601  LATERAL BOUNDARY-CONDITIONS, Mon. Weather Rev., 121, 2814-2832,
602  https://doi.org/10.1175/1520-0493(1993)121<2814:Doasgr>2.0.Co;2, 1993.

603 Giorgi, F., Pal, J. S., Bi, X., Sloan, L., Elguindi, N., and Solmon, F.: Introduction to the TAC special issue: The
604  RegCNET network, Theor. Appl. Climatol., 86, 1-4, https://doi.org/10.1007/s00704-005-0199-z, 2006.

605 Giorgi, F., Coppola, E., Solmon, F., Mariotti, L., Sylla, M. B., Bi, X., Elguindi, N., Diro, G. T.*, et al.*: RegCM4:
606  model description and preliminary tests over multiple CORDEX domains, Clim. Res., 52, 7-29,
607  https://doi.org/10.3354/cr01018, 2012.

608 Guenther, A., Hewitt, C. N., Erickson, D., Fall, R., Geron, C., Graedel, T., Harley, P., Klinger, L.*, et al.*: A
609  Global-Model of Natural Volatile Organic-Compound Emissions, J. Geophys. Res.: Atmos., 100,
610  8873-8892, https://doi.org/10.1029/94jd02950, 1995.

611 Han, Z. W., Li, J. W., Xia, X. G., and Zhang, R. J.: Investigation of direct radiative effects of aerosols in dust
612  storm season over East Asia with an online coupled regional climate-chemistry-aerosol model, Atmos.
613  Environ., 54, 688-699, https://doi.org/10.1016/j.atmosenv.2012.01.041, 2012.

614 Han, Z. W., Xie, Z. X., Wang, G. H., Zhang, R. J., and Tao, J.: Modeling organic aerosols over east China using
615  a volatility basis-set approach with aging mechanism in a regional air quality model, Atmos. Environ., 124,
616  186-198, https://doi.org/10.1016/j.atmosenv.2015.05.045, 2016.

617 He, M. Z., Kimball, J. S., Maneta, M. P., Maxwell, B. D., Moreno, A., Begueria, S., and Wu, X. C.: Regional
618  Crop Gross Primary Productivity and Yield Estimation Using Fused Landsat-MODIS Data, Remote Sens.,
619  10, https://doi.org/10.3390/rs10030372, 2018.

620 Hong, C. P., Zhang, Q., Zhang, Y., Davis, S. J., Tong, D., Zheng, Y. X., Liu, Z., Guan, D. B.*, et al.*: Impacts of
621  climate change on future air quality and human health in China, Proc. Natl. Acad. Sci. U.S.A., 116,
622  17193-17200, https://doi.org/10.1073/pnas.1812881116, 2019.

623 Horowitz, L. W., Walters, S., Mauzerall, D. L., Emmons, L. K., Rasch, P. J., Granier, C., Tie, X. X., Lamarque, J.
624  F.*, et al.*: A global simulation of tropospheric ozone and related tracers: Description and evaluation of
625  MOZART, version 2, J. Geophys. Res.: Atmos., 108, https://doi.org/10.1029/2002jd002853, 2003.

626 Kan, H. D., Chen, R. J., and Tong, S. L.: Ambient air pollution, climate change, and population health in China,

627   Environ. Int., 42, 10-19, https://doi.org/10.1016/j.envint.2011.03.003, 2012.

628   Kiehl, J. T., Hack, J. J., Bonan, G. B., Boville, B. A., and Briegleb, B. P.: Description of the NCAR community
629   climate model (CCM3), National Center for Atmospheric Research, Boulder, CO (United States). Climate
630   and Global Dynamics Div., Technical Report PB-97-131528/XAB;NCAR/TN-420-STR TRN: 70341499,
631   1996.

632   Kim, K. H., Kabir, E., and Kabir, S.: A review on the human health impact of airborne particulate matter,
633   Environ. Int., 74, 136-143, https://doi.org/10.1016/j.envint.2014.10.005, 2015.

634   Kou, X. X., Zhang, M. G., Peng, Z., and Wang, Y. H.: Assessment of the biospheric contribution to surface
635   atmospheric CO_2 concentrations over East Asia with a regional chemical transport model, Adv. Atmos. Sci.,
636   32, 287-300, https://doi.org/10.1007/s00376-014-4059-6, 2015.

637   Lamarque, J. F., Dentener, F., McConnell, J., Ro, C. U., Shaw, M., Vet, R., Bergmann, D., Cameron-Smith, P., *et*
638   *al.*: Multi-model mean nitrogen and sulfur deposition from the Atmospheric Chemistry and Climate Model
639   Intercomparison Project (ACCMIP): evaluation of historical and projected future changes, Atmos. Chem.
640   Phys., 13, 7997-8018, https://doi.org/10.5194/acp-13-7997-2013, 2013.

641   Lawrence, P. J. and Chase, T. N.: Representing a new MODIS consistent land surface in the Community Land
642   Model (CLM 3.0), J. Geophys. Res.: Biogeosci., 112, https://doi.org/10.1029/2006jg000168, 2007.

643   Li, B., Gasser, T., Ciais, P., Piao, S., Tao, S., Balkanski, Y., Hauglustaine, D., Boisier, J.-P., *et al.*: The
644   contribution of China's emissions to global climate forcing, Nature, 531, 357-361,
645   https://doi.org/10.1038/nature17165, 2016a.

646   Li, J. W., Han, Z. W., and Xie, Z. X.: Model analysis of long-term trends of aerosol concentrations and direct
647   radiative forcings over East Asia, Tellus B: Chem. Phys. Meteorol., 65,
648   https://doi.org/10.3402/tellusb.v65i0.20410, 2013a.

649   Li, J. W., Han, Z. W., and Zhang, R. J.: Influence of aerosol hygroscopic growth parameterization on aerosol
650   optical depth and direct radiative forcing over East Asia, Atmos. Res., 140, 14-27,
651   https://doi.org/10.1016/j.atmosres.2014.01.013, 2014.

652   Li, M., Wang, T., Han, Y., Xie, M., Li, S., Zhuang, B., and Chen, P.: Modeling of a severe dust event and its
653   impacts on ozone photochemistry over the downstream Nanjing megacity of eastern China, Atmos.
654   Environ., 160, 107-123, https://doi.org/10.1016/j.atmosenv.2017.04.010, 2017a.

655   Li, M., Zhang, Q., Kurokawa, J., Woo, J. H., He, K. B., Lu, Z. F., Ohara, T., Song, Y., *et al.*: MIX: a mosaic
656   Asian anthropogenic emission inventory under the international collaboration framework of the MICS-Asia
657   and HTAP, Atmos. Chem. Phys., 17, 935-963, https://doi.org/10.5194/acp-17-935-2017, 2017b.

658   Li, S., Wang, T. J., Zhuang, B. L., and Han, Y.: Indirect radiative forcing and climatic effect of the anthropogenic
659   nitrate aerosol on regional climate of China, Adv. Atmos. Sci., 26, 543-552,
660   https://doi.org/10.1007/s00376-009-0543-9, 2009.

661   Li, S., Wang, T. J., Solmon, F., Zhuang, B. L., Wu, H., Xie, M., Han, Y., and Wang, X. M.: Impact of aerosols on
662   regional climate in southern and northern China during strong/weak East Asian summer monsoon years, J.
663   Geophys. Res.: Atmos., 121, 4069-4081, https://doi.org/10.1002/2015jd023892, 2016b.

664   Li, X. L., Liang, S. L., Yu, G. R., Yuan, W. P., Cheng, X., Xia, J. Z., Zhao, T. B., Feng, J. M., *et al.*: Estimation
665   of gross primary production over the terrestrial ecosystems in China, Ecol. Model., 261, 80-92,
666   https://doi.org/10.1016/j.ecolmodel.2013.03.024, 2013b.

667   Liu, L., Solmon, F., Vautard, R., Hamaoui-Laguel, L., Torma, C. Z., and Giorgi, F.: Ragweed pollen production
668   and dispersion modelling within a regional climate system, calibration and application over Europe,
669   Biogeosciences, 13, 2769-2786, https://doi.org/10.5194/bg-13-2769-2016, 2016.

670   Liu, Z., Deng, Z., He, G., Wang, H. L., Zhang, X., Lin, J., Qi, Y., and Liang, X.: Challenges and opportunities

671   for carbon neutrality in China, Nat Rev Earth Env, 3, 141-155, https://doi.org/10.1038/s43017-021-00244-x,
672   2022.

673   Lu, X., Zhang, S. J., Xing, J., Wang, Y. J., Chen, W. H., Ding, D., Wu, Y., Wang, S. X.*, et al.*: Progress of Air

674   Pollution Control in China and Its Challenges and Opportunities in the Ecological Civilization Era,

675   Engineering, 6, 1423-1431, https://doi.org/10.1016/j.eng.2020.03.014, 2020.

676   Lu, X. L., Chen, M., Liu, Y. L., Miralles, D. G., and Wang, F. M.: Enhanced water use efficiency in global

677   terrestrial ecosystems under increasing aerosol loadings, Agric. For. Meteorol., 237, 39-49,

678   https://doi.org/10.1016/j.agrformet.2017.02.002, 2017.

679   Ma, D., Wang, T., Wu, H., Qu, Y., Liu, J., Liu, J., Li, S., Zhuang, B.*, et al.*: The effect of anthropogenic emission,

680   meteorological factors, and carbon dioxide on the surface ozone increase in China from 2008 to 2018

681   during the East Asia summer monsoon season, Atmos. Chem. Phys., 23, 6525-6544,

682   https://doi.org/10.5194/acp-23-6525-2023, 2023a.

683   Ma, D. Y., Wang, T. J., Xu, B. Y., Song, R., Gao, L. B., Chen, H. M., Ren, X. J., Li, S.*, et al.*: The mutual

684   interactions among ozone, fine particulate matter, and carbon dioxide on summer monsoon climate in East

685   Asia, Atmos. Environ., 299, https://doi.org/10.1016/j.atmosenv.2023.119668, 2023b.

686   Madani, N., Kimball, J. S., Affleck, D. L. R., Kattge, J., Graham, J., van Bodegom, P. M., Reich, P. B., and

687   Running, S. W.: Improving ecosystem productivity modeling through spatially explicit estimation of

688   optimal light use efficiency, J. Geophys. Res.: Biogeosci., 119, 1755-1769,

689   https://doi.org/10.1002/2014jg002709, 2014.

690   Madronich, S. and Flocke, S.: The role of solar radiation in atmospheric chemistry, Environ. Chem., 1-26,

691   https://doi.org/10.1007/978-3-540-69044-3_1, 1998.

692   Niinemets, Ü., Tenhunen, J. D., Harley, P. C., and Steinbrecher, R.: A model of isoprene emission based on

693   energetic requirements for isoprene synthesis and leaf photosynthetic properties for Liquidambar and

694   Quercus, Plant, Cell & Environment, 22, 1319-1335, https://doi.org/10.1046/j.1365-3040.1999.00505.x,

695   2002.

696   Oleson, K. W., Niu, G. Y., Yang, Z. L., Lawrence, D. M., Thornton, P. E., Lawrence, P. J., Stockli, R., Dickinson,

697   R. E.*, et al.*: Improvements to the Community Land Model and their impact on the hydrological cycle, J.

698   Geophys. Res.: Biogeosci., 113, https://doi.org/10.1029/2007jg000563, 2008.

699   Pacifico, F., Harrison, S. P., Jones, C. D., Arneth, A., Sitch, S., Weedon, G. P., Barkley, M. P., Palmer, P. I., et al.:

700   Evaluation of a photosynthesis-based biogenic isoprene emission scheme in JULES and simulation of

701   isoprene emissions under present-day climate conditions, Atmos. Chem. Phys., 11, 4371-4389,

702   https://doi.org/10.5194/acp-11-4371-2011, 2011.

703   Pal, J. S., Giorgi, F., Bi, X. Q., Elguindi, N., Solmon, F., Gao, X. J., Rauscher, S. A., Francisco, R.*, et al.*:

704   Regional climate modeling for the developing world - The ICTP RegCM3 and RegCNET, Bull. Am.

705   Meteorol. Soc., 88, 1395-+, https://doi.org/10.1175/Bams-88-9-1395, 2007.

706   Peters, W., Jacobson, A. R., Sweeney, C., Andrews, A. E., Conway, T. J., Masarie, K., Miller, J. B., Bruhwiler, L.

707   M. P.*, et al.*: An atmospheric perspective on North American carbon dioxide exchange: CarbonTracker,

708   Proc. Natl. Acad. Sci. U.S.A., 104, 18925-18930, https://doi.org/10.1073/pnas.0708986104, 2007.

709   Pu, X., Wang, T. J., Huang, X., Melas, D., Zanis, P., Papanastasiou, D. K., and Poupkou, A.: Enhanced surface

710   ozone during the heat wave of 2013 in Yangtze River Delta region, China, Sci. Total Environ., 603,

711   807-816, https://doi.org/10.1016/j.scitotenv.2017.03.056, 2017.

712   Reynolds, R. W., Rayner, N. A., Smith, T. M., Stokes, D. C., and Wang, W. Q.: An improved in situ and satellite

713   SST analysis for climate, J. Clim., 15, 1609-1625,

714   https://doi.org/10.1175/1520-0442(2002)015<1609:Aiisas>2.0.Co;2, 2002.

Running, S. W.: A Measurable Planetary Boundary for the Biosphere, Science, 337, 1458-1459, https://doi.org/10.1126/science.1227620, 2012.

Scheuch, M., Hoper, D., and Beer, M.: RIEMS: a software pipeline for sensitive and comprehensive taxonomic classification of reads from metagenomics datasets, BMC Bioinf., 16, https://doi.org/10.1186/s12859-015-0503-6, 2015.

Shalaby, A., Zakey, A. S., Tawfik, A. B., Solmon, F., Giorgi, F., Stordal, F., Sillman, S., Zaveri, R. A., *et al.*: Implementation and evaluation of online gas-phase chemistry within a regional climate model (RegCM-CHEM4), Geosci. Model Dev., 5, 741-760, https://doi.org/10.5194/gmd-5-741-2012, 2012.

Shindell, D. T., Lamarque, J. F., Schulz, M., Flanner, M., Jiao, C., Chin, M., Young, P. J., Lee, Y. H., *et al.*: Radiative forcing in the ACCMIP historical and future climate simulations, Atmos. Chem. Phys., 13, 2939-2974, https://doi.org/10.5194/acp-13-2939-2013, 2013.

Sitch, S., Cox, P. M., Collins, W. J., and Huntingford, C.: Indirect radiative forcing of climate change through ozone effects on the land-carbon sink, Nature, 448, 791-U794, https://doi.org/10.1038/nature06059, 2007.

Slingo, A.: A Gcm Parameterization for the Shortwave Radiative Properties of Water Clouds, J. Atmos. Sci., 46, 1419-1427, https://doi.org/10.1175/1520-0469(1989)046<1419:Agpfts>2.0.Co;2, 1989.

Small, E. E., Sloan, L. C., Hostetler, S., and Giorgi, F.: Simulating the water balance of the Aral Sea with a coupled regional climate-lake model, J. Geophys. Res.: Atmos., 104, 6583-6602, https://doi.org/Doi 10.1029/98jd02348, 1999.

Solmon, F., Elguindi, N., and Mallet, M.: Radiative and climatic effects of dust over West Africa, as simulated by a regional climate model, Clim. Res., 52, 97-113, https://doi.org/10.3354/cr01039, 2012.

Solmon, F., Giorgi, F., and Liousse, C.: Aerosol modelling for regional climate studies: application to anthropogenic particles and evaluation over a European/African domain, Tellus B: Chem. Phys. Meteorol., 58, 51-72, https://doi.org/10.1111/j.1600-0889.2005.00155.x, 2006.

Spitters, C. J. T., Toussaint, H., and Goudriaan, J.: SEPARATING THE DIFFUSE AND DIRECT COMPONENT OF GLOBAL RADIATION AND ITS IMPLICATIONS FOR MODELING CANOPY PHOTOSYNTHESIS .1. COMPONENTS OF INCOMING RADIATION, Agric. For. Meteorol., 38, 217-229, https://doi.org/10.1016/0168-1923(86)90060-2, 1986.

Strada, S. and Unger, N.: Potential sensitivity of photosynthesis and isoprene emission to direct radiative effects of atmospheric aerosol pollution, Atmos. Chem. Phys., 16, 4213-4234, https://doi.org/10.5194/acp-16-4213-2016, 2016.

Turuncoglu, U. U., Dalfes, N., Murphy, S., and DeLuca, C.: Toward self-describing and workflow integrated Earth system models: A coupled atmosphere-ocean modeling system application, Environ. Model. Software, 39, 247-262, https://doi.org/10.1016/j.envsoft.2012.02.013, 2013.

Wang, T., Xue, L. K., Brimblecombe, P., Lam, Y. F., Li, L., and Zhang, L.: Ozone pollution in China: A review of concentrations, meteorological influences, chemical precursors, and effects, Sci. Total Environ., 575, 1582-1596, https://doi.org/10.1016/j.scitotenv.2016.10.081, 2017.

Wang, T. J., Li, S., Shen, Y., Deng, J. J., and Xie, M.: Investigations on direct and indirect effect of nitrate on temperature and precipitation in China using a regional climate chemistry modeling system, J. Geophys. Res.: Atmos., 115, https://doi.org/10.1029/2009jd013264, 2010.

Wesely, M. L.: Parameterization of Surface Resistances to Gaseous Dry Deposition in Regional-Scale Numerical-Models, Atmos. Environ., 23, 1293-1304, https://doi.org/10.1016/0004-6981(89)90153-4, 1989.

Wiedinmyer, C., Akagi, S. K., Yokelson, R. J., Emmons, L. K., Al-Saadi, J. A., Orlando, J. J., and Soja, A. J.: The Fire INventory from NCAR (FINN): a high resolution global model to estimate the emissions from open burning, Geosci. Model Dev., 4, 625-641, https://doi.org/10.5194/gmd-4-625-2011, 2011.

Xie, X. D., Wang, T. J., Yue, X., Li, S., Zhuang, B. L., and Wang, M. H.: Effects of atmospheric aerosols on terrestrial carbon fluxes and CO2 concentrations in China, Atmos. Res., 237, https://doi.org/10.1016/j.atmosres.2020.104859, 2020.

Xie, X. D., Wang, T. J., Yue, X., Li, S., Zhuang, B. L., Wang, M. H., and Yang, X. Q.: Numerical modeling of ozone damage to plants and its effects on atmospheric CO2 in China, Atmos. Environ., 217, https://doi.org/10.1016/j.atmosenv.2019.116970, 2019.

Xiong, Z., Fu, C. B., and Yan, X. D.: Regional integrated environmental model system and its simulation of East Asia summer monsoon, Chin. Sci. Bull., 54, 4253-4261, https://doi.org/10.1007/s11434-009-0669-2, 2009.

Xu, B. Y., Wang, T. J., Ma, D. Y., Song, R., Zhang, M., Gao, L. B., Li, S., Zhuang, B. L., *et al.*: Impacts of regional emission reduction and global climate change on air quality and temperature to attain carbon neutrality in China, Atmos. Res., 279, https://doi.org/10.1016/j.atmosres.2022.106384, 2022.

Xu, B. Y., Wang, T. J., Gao, L. B., Ma, D. Y., Song, R., Zhao, J., Yang, X. G., Li, S., *et al.*: Impacts of meteorological factors and ozone variation on crop yields in China concerning carbon neutrality objectives in 2060, Environ. Pollut., 317, https://doi.org/10.1016/j.envpol.2022.120715, 2023.

Yahya, K., Wang, K., Campbell, P., Chen, Y., Glotfelty, T., He, J., Pirhalla, M., and Zhang, Y.: Decadal application of WRF/Chem for regional air quality and climate modeling over the U.S. under the representative concentration pathways scenarios. Part 1: Model evaluation and impact of downscaling, Atmos. Environ., 152, 562-583, https://doi.org/10.1016/j.atmosenv.2016.12.029, 2017.

Yin, C. Q., Wang, T. J., Solmon, F., Mallet, M., Jiang, F., Li, S., and Zhuang, B. L.: Assessment of direct radiative forcing due to secondary organic aerosol over China with a regional climate model, Tellus Series B-Chemical and Physical Meteorology, 67, https://doi.org/10.3402/tellusb.v67.24634, 2015.

Yin, J. F., Wang, D. H., Zhai, G. Q., and Xu, H. B.: An investigation into the relationship between liquid water content and cloud number concentration in the stratiform clouds over north China, Atmos. Res., 139, 137-143, https://doi.org/10.1016/j.atmosres.2013.12.004, 2014.

Young, P. J., Archibald, A. T., Bowman, K. W., Lamarque, J. F., Naik, V., Stevenson, D. S., Tilmes, S., Voulgarakis, A., *et al.*: Pre-industrial to end 21st century projections of tropospheric ozone from the Atmospheric Chemistry and Climate Model Intercomparison Project (ACCMIP), Atmos. Chem. Phys., 13, 2063-2090, https://doi.org/10.5194/acp-13-2063-2013, 2013.

Yue, X. and Unger, N.: The Yale Interactive terrestrial Biosphere model version 1.0: description, evaluation and implementation into NASA GISS ModelE2, Geosci. Model Dev., 8, 2399-2417, https://doi.org/10.5194/gmd-8-2399-2015, 2015.

Yue, X. and Unger, N.: Aerosol optical depth thresholds as a tool to assess diffuse radiation fertilization of the land carbon uptake in China, Atmos. Chem. Phys., 17, 1329-1342, https://doi.org/10.5194/acp-17-1329-2017, 2017.

Yue, X., Strada, S., Unger, N., and Wang, A. H.: Future inhibition of ecosystem productivity by increasing wildfire pollution over boreal North America, Atmos. Chem. Phys., 17, 13699-13719, https://doi.org/10.5194/acp-17-13699-2017, 2017.

Zakey, A. S., Solmon, F., and Giorgi, F.: Implementation and testing of a desert dust module in a regional climate model, Atmos. Chem. Phys., 6, 4687-4704, https://doi.org/10.5194/acp-6-4687-2006, 2006.

Zaveri, R. A. and Peters, L. K.: A new lumped structure photochemical mechanism for large-scale applications, J. Geophys. Res.: Atmos., 104, 30387-30415, https://doi.org/10.1029/1999jd900876, 1999.

Zhang, H., Jing, X., and Li, J.: Application and evaluation of a new radiation code under McICA scheme in BCC_AGCM2.0.1, Geosci. Model Dev., 7, 737-754, https://doi.org/10.5194/gmd-7-737-2014, 2014.

Zhang, H., Wang, Z. L., Wang, Z. Z., Liu, Q. X., Gong, S. L., Zhang, X. Y., Shen, Z. P., Lu, P., *et al.*: Simulation

803   of direct radiative forcing of aerosols and their effects on East Asian climate using an interactive
804   AGCM-aerosol coupled system, Clim. Dyn., 38, 1675-1693, https://doi.org/10.1007/s00382-011-1131-0,
805   2012.

806 Zheng, B., Tong, D., Li, M., Liu, F., Hong, C. P., Geng, G. N., Li, H. Y., Li, X.*, et al.*: Trends in China's
807   anthropogenic emissions since 2010 as the consequence of clean air actions, Atmos. Chem. Phys., 18,
808   14095-14111, https://doi.org/10.5194/acp-18-14095-2018, 2018.

809 Zhou, Y., Huang, A. N., Jiang, J., and La, M. K.: Modeled interaction between the subseasonal evolving of the
810   East Asian summer monsoon and the direct effect of anthropogenic sulfate, J. Geophys. Res.: Atmos., 119,
811   1993-2016, https://doi.org/10.1002/2013jd020612, 2014.

812 Zhuang, B. L., Jiang, F., Wang, T. J., Li, S., and Zhu, B.: Investigation on the direct radiative effect of fossil fuel
813   black-carbon aerosol over China, Theor. Appl. Climatol., 104, 301-312,
814   https://doi.org/10.1007/s00704-010-0341-4, 2011.

815 Zhuang, B. L., Li, S., Wang, T. J., Deng, J. J., Xie, M., Yin, C. Q., and Zhu, J. L.: Direct radiative forcing and
816   climate effects of anthropogenic aerosols with different mixing states over China, Atmos. Environ., 79,
817   349-361, https://doi.org/10.1016/j.atmosenv.2013.07.004, 2013.

818 Zhuang, B. L., Li, S., Wang, T. J., Liu, J., Chen, H. M., Chen, P. L., Li, M. M., and Xie, M.: Interaction between
819   the Black Carbon Aerosol Warming Effect and East Asian Monsoon Using RegCM4, J. Clim., 31,
820   9367-9388, https://doi.org/10.1175/Jcli-D-17-0767.1, 2018.

821